Letter

Metal-insulator transition in infinitesimally weakly disordered flat bands

Tilen Čadež*
Center for Theoretical Physics of Complex Systems, Institute for Basic Science (IBS), Daejeon 34126, Republic of Korea

Yeongjun Kim,† Alexei Andreanov,‡ and Sergej Flach§
Center for Theoretical Physics of Complex Systems, Institute for Basic Science (IBS), Daejeon 34126, Republic of Korea and Basic Science Program, Korea University of Science and Technology (UST), Daejeon 34113, Republic of Korea

(Received 26 July 2021; revised 29 October 2021; accepted 2 November 2021; published 15 November 2021)

We study the effect of infinitesimal onsite disorder on d-dimensional all bands flat lattices. The lattices are generated from diagonal Hamiltonians by a sequence of $(d+1)$ local unitary transformations parametrized by angles θ_i. Without loss of generality, we consider the case of two flat bands separated by a finite gap, Δ. The perturbed states originating from the flat bands are described by an effective tight-binding network with finite on- and off-diagonal disorder strength which depends on the manifold angles θ_i. The original infinitesimal on-site disorder strength W is only affecting the overall scale of the effective Hamiltonian. Upon variation of the manifold angles for $d=1$ and $d=2$ we find that localization persists for any choice of local unitaries, and the localization length can be maximized for specific values of θ_i. Instead, in $d=3$ we identify a nonperturbative metal-insulator transition upon varying all bands' flat manifold angles.

DOI: 10.1103/PhysRevB.104.L180201

Introduction. A peculiar feature of some tight-binding Hamiltonian systems is the existence of dispersionless bands known as *flat bands* [1–5]. Due to destructive interference and macroscopic degeneracy of such systems one can construct eigenstates which occupy only a finite number of lattice sites, called *compact localized states* (CLSs) [6,7]. The interest in flat-band systems is motivated by their high sensitivity to perturbations, such as interactions or disorder, that can lead to various interesting physical phenomena in their presence: ground state ferromagnetism [1,8–11], superfluidity and superconductivity [12–16], many-body localization [17,18], and unconventional Anderson localization [19,20].

In this Letter we consider the impact of infinitesimally weak disorder on flat bands. Localization in weakly disordered flat-band systems has been previously studied by several authors [20–27]. When some of the bands have been dispersive and flat bands have been gapped away from the dispersive bands, the independence of localization properties on a weak disorder strength has been reported [21–25,27] and effective low-energy models have been derived for the case of the two-dimensional $\mathcal{T}_3$ (dice) lattice [21] and planar pyrochlore lattice [23]. On the other hand, when a flat band is immersed into a dispersive band, weak disorder leads to a diverging localization length, with a variety of unconventional exponents [20,24,25]. The particular case, when a dispersive band touches a flat band, might lead to the emergence of critical states arising from the flat-band states [23].

What happens when all bands turn flat—all bands flat (ABF) systems—where *all* bands are dispersionless? In the presence of disorder there are three distinct regimes of disorder strength: the (infinitesimally) weak—the disorder strength is much smaller than the gaps between the flat-band energies, and the intermediate one—the two energy scales are comparable and the strong disorder regime. In the intermediate regime the flat bands hybridize due to the disorder and this can lead to delocalization and an inverse Anderson transition [28], whereas the strong regime always leads to Anderson localization. For weak disorder we expect nonperturbative effects due to the interplay of the disorder and the macroscopic degeneracy of the flat band. A metallic phase and a mobility edge around the flat-band energy has been numerically observed for weak disorder in a fine-tuned three-dimensional eight-band ABF system [22].

We systematically construct ABF systems in one, two, and three dimensions through local unitary transformations. We then reveal the effect of (infinitesimally) weak on-site disorder by deriving the underlying scale-free effective Hamiltonian. We illustrate for the simplest case of two bands that infinitesimally weak disorder in one and two dimensions does not lead to delocalization. In three-dimensional systems we demonstrate a metal-insulator transition, which is driven by the variation of the parameters of the local unitary transformations. There is, in general, a mobility edge in the metallic phase.

Construction of all bands flat Hamiltonians. A systematic way to generate ABF lattices is based on the observation that *any* ν-band ABF system is represented by a macroscopically degenerate diagonal matrix $\mathcal{H}_{\rm FD}$ [20,29] after diagonalization. Since unitary transformations do not change the spectrum, *any* (local or nonlocal) unitary transformation applied to $\mathcal{H}_{\rm FD}$

*tilencadez@ibs.re.kr
†yeongjun@ust.ac.kr
‡aalexei@ibs.re.kr
§sflach@ibs.re.kr

produces an ABF Hamiltonian with the same spectrum. We denote the basis where the Hamiltonian is diagonal as *fully detangled* (FD), while the basis after the unitary transformation is denoted as *fully entangled* (FE) [20]. We limit our consideration to local unitary transformations (LUTs)—in the one-dimensional (1D) case the LUT based construction is exhaustive for short-range hopping ABF Hamiltonians [29]. In the simplest setting LUTs connect the ν bands in either one or, at most, two adjacent unit cells. In that case the general local unitary transformations are given by SU(ν) matrices, each of which is parametrized by $\nu^2 - 1$ real parameters. In a d-dimensional system one would need at least $d + 1$ LUT in order to ensure connectivity of the final Hamiltonian. We denote the corresponding total unitary transformation by $\mathcal{U}$ and the transformed Hamiltonian $\mathcal{H}$ is then given as

$$\mathcal{H} = \mathcal{U}\mathcal{H}_{\rm FD}\mathcal{U}^\dagger. \tag{1}$$

In the examples presented below, we focus on the simplest nontrivial, $\nu = 2$ band case. The Hamiltonian in the FD basis is diagonal and given by

$$\mathcal{H}_{\rm FD} = \Delta/2 \sum_{\mathbf{e}} |a_{\mathbf{e}}^{(0)}\rangle\langle a_{\mathbf{e}}^{(0)}| - |b_{\mathbf{e}}^{(0)}\rangle\langle b_{\mathbf{e}}^{(0)}|,$$

where the sum runs over all the unit cells $\mathbf{e} = ne_x$, $\mathbf{e} = ne_x + me_y$, and $\mathbf{e} = ne_x + me_y + le_z$ for $d = 1, 2$, and 3 and integers n, m, and l, respectively. Each LUT can then be written as

$$\mathcal{U}_i = \sum_{\mathbf{e}} \big(z_i |a_{\mathbf{e}}^{(i)}\rangle\langle a_{\mathbf{e}}^{(i-1)}| + w_i |a_{\mathbf{e}}^{(i)}\rangle\langle b_{\mathbf{e}'}^{(i-1)}| - w_i^* |b_{\mathbf{e}'}^{(i)}\rangle\langle a_{\mathbf{e}}^{(i-1)}| + z_i^* |b_{\mathbf{e}'}^{(i)}\rangle\langle b_{\mathbf{e}'}^{(i-1)}|\big), \tag{2}$$

where i denotes the ith LUT, $a_{\mathbf{e}}^{(i)}$ and $b_{\mathbf{e}}^{(i)}$ are the two orbitals within a unit cell $\mathbf{e}$ in a basis after the ith LUT, $\mathbf{e}' = \mathbf{e}$ for $i = 1$, $\mathbf{e}' = \mathbf{e} - e_x$ for $i = 2$, $\mathbf{e}' = \mathbf{e} - e_y$ for $i = 3$, $\mathbf{e}' = \mathbf{e} - e_z$ for $i = 4$, $z_i = \cos\theta_i\, e^{i\varphi_i}$, and $w_i = \sin\theta_i\, e^{i\bar{\varphi}_i}$.

The one-dimensional case construction is schematically shown in Figs. 1(a)–1(c). Figure 1(a) shows the FD basis, with circles representing disconnected sites. The CLSs in this basis occupy a single site. We first apply the LUT $\mathcal{U}_1$ within a unit cell as shown in Fig. 1(a) and then apply a second LUT, $\mathcal{U}_2$—the sites affected by the LUT are indicated by the blue shaded areas on the panels. This procedure introduces hopping matrix elements within and between the adjacent unit cells, as schematically shown in Fig. 1(c). In this case we then have $\mathcal{U} = \mathcal{U}_2\mathcal{U}_1$. This construction includes the well-known Creutz ladder in a magnetic field [30] where ABF appear at half flux quantum per plaquette. It is obtained [29] for $\Delta = 4t_c$, $\theta_1 = \theta_2 = \pi/4$, $\varphi_1 = -\bar{\varphi}_1$ and $\varphi_2 = \pi/2$, $\bar{\varphi}_2 = 0$. Here t_c is the diagonal hopping element in the Creutz ladder.

In a two-dimensional case the procedure is a natural extension of the one-dimensional case, with the second LUT connecting the adjacent unit cells along one direction (here chosen as the x direction). Then one applies a third LUT, $\mathcal{U}_3$, which connects the adjacent unit cells along the y direction and $\mathcal{U} = \mathcal{U}_3\mathcal{U}_2\mathcal{U}_1$. Similarly in the three-dimensional case one adds the fourth LUT, $\mathcal{U}_4$, to obtain $\mathcal{U} = \mathcal{U}_4\mathcal{U}_3\mathcal{U}_2\mathcal{U}_1$.

Scale-free model in weak disorder. In the fully entangled basis we add a random on-site potential disorder, $\varepsilon_{\mathbf{e},o}$, in the orbital $o = p$ and f of the unit cell $\mathbf{e}$ and we use the fully entangled basis labels as $p = a_{\mathbf{e}}^{(d+1)}$ and $f = b_{\mathbf{e}}^{(d+1)}$—for simplicity we consider box disorder, that is, $\varepsilon_{\mathbf{e},o} \in [-W/2, W/2]$, where W is the strength of the disorder. Our conclusions hold for other distributions with finite support as well. The Hamiltonian for the on-site disorder is then $\mathcal{H}_d = WD$, where D is a diagonal matrix with *all* nonzero elements drawn at random from $[-1/2, 1/2]$. This is schematically depicted in Fig. 1(c) by red arrows. Next we perform the inverse transformation $\mathcal{U}^\dagger$ into the original FD basis and write the total Hamiltonian in the FD basis as $\mathcal{H}_{\rm tot} = \mathcal{H}_{\rm FD} + W\,\mathcal{U}^\dagger D\mathcal{U}$. We are interested in the (infinitesimally) weak disorder $W \ll \Delta$. Therefore the first term $\mathcal{H}_{\rm FD}$ in the total Hamiltonian is much larger than the second term, while at the same time it is composed of two flat bands. It follows from degenerate perturbation theory that weak perturbations will keep the eigenvalues close to a flat band and the eigenstates will in leading order be composed of the eigenvectors from the unperturbed Hilbert subspace which corresponds to the chosen flat-band energy. Hence, we can project onto one of the flat bands using the projection operator $P_a = \sum_{\mathbf{e}} |a_{\mathbf{e}}\rangle\langle a_{\mathbf{e}}|$, effectively removing the other flat band completely. It is worth pointing out that this projector is compact in our case [31]. We introduce a shorthand notation of $|a_{\mathbf{e}}\rangle \equiv |a_{\mathbf{e}}^{(0)}\rangle$ for states in the FD basis. After the projection the $\mathcal{H}_{\rm FD}$ term in the total Hamiltonian becomes a trivial constant shift of energy, corresponding to the chosen flat-band energy. Thus all we are left with is the second term due to the on-site disorder. The projected Hamiltonian can thus be written as

$$\mathcal{H}_P = W\,\mathcal{H}_{\rm sf}, \tag{3}$$

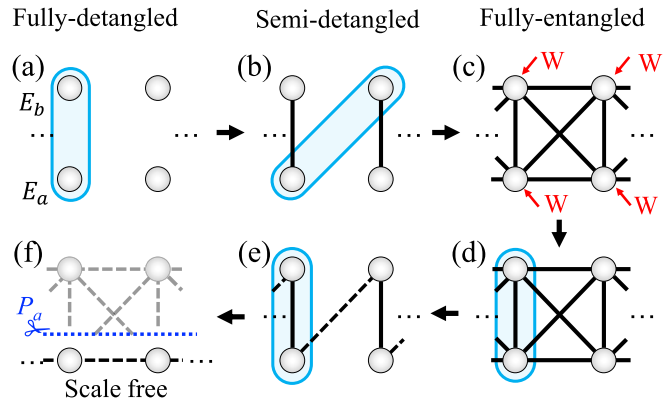

FIG. 1. One-dimensional two-band ABF system. (a) FD basis with disconnected sites. The first LUT, $\mathcal{U}_1$, applied within a unit cell (indicated by blue shaded area) leads to panel (b) where the second LUT, $\mathcal{U}_2$, is applied between two nearest unit cells (again indicated by the blue shaded area), leading to panel (c). We apply on-site potential disorder on the sites marked by arrows and then disentangle with $\mathcal{U}_2^\dagger$ as indicated in panel (d). This leads to panel (e) and gives rise to an effective dimerized one-dimensional chain, with every second hopping element (dashed lines) being random; further disentangling with $\mathcal{U}_1^\dagger$ brings us back to an initial FD basis, but due to disorder random hopping matrix elements of the order of disorder strength W appear within and between the nearest unit cells. (f) In a weakly disordered case we project to one of the flat bands (as marked by the blue dashed line and scissors) and obtain an effective scale-free single-band model.

where we defined the *scale-free Hamiltonian* $\mathcal{H}_{\rm sf} = P_a\mathcal{U}^\dagger D\mathcal{U}P_a$—the only remaining energy scale W appears just as a total prefactor. This scale-free form of the projected Hamiltonian explains the *independence* of the localization properties reported in previous studies of flat-band systems in the weak disorder regime [21–25,27] and is one of the main results of this work. This scale-free model is the base for the analysis of the localization properties of the weakly disordered models discussed below.

Weak disorder effects in $d = 1$ and $d = 2$. For the one-dimensional case the inverse transformation after introducing the on-site disorder W is schematically shown in Figs. 1(d) and 1(e), while the projection onto the chosen flat band is depicted in Fig. 1(f). The scale-free Hamiltonian in this case corresponds to the 1D Anderson model with correlated disorder in both on-site energies and nearest-neighbor hoppings and is

$$\mathcal{H}_{\rm sf} = \sum_n (V_n|a_n\rangle\langle a_n| + t_n|a_{n+1}\rangle\langle a_n| + \text{H.c.}), \qquad (4)$$

where V_n and t_n are functions of LUT manifold angles and the disorder realization.

We evaluate the impact of infinitesimal disorder on the ABF model and study the localization properties of the scale-free Hamiltonians (4). As a check we also make sure that the results match those obtained from the full Hamiltonian $\mathcal{H}_{\rm tot}$. We analyze the participation number (PN) of an eigenstate, which contains information on the localization properties of that eigenstate. The PN of an eigenstate μ is defined as [32–34] $\text{PN}_\mu = (\sum_{\mathbf{e}} \psi^4_{\mu,\mathbf{e}})^{-1}$, where $\psi_{\mu,\mathbf{e}}$ is the coefficient of the eigenstate in a chosen basis. We calculate it via the exact diagonalization (ED) in the FD real space basis [as presented in Fig. 1(f) for the 1D case]. The localization properties are extracted from the scaling of the average PN with the system size $\langle\text{PN}\rangle \sim L^\alpha$, where $\alpha = 0$ and $\alpha = d$ (d being the dimension of the system) indicate localized and extended states, respectively.

The on-site potential energies and hopping elements in Eq. (4) are $V_n = (\varepsilon_{n,p}\cos^2\theta_2 + \varepsilon_{n,f}\sin^2\theta_2)\cos^2\theta_1 + (\varepsilon_{n+1,f}\cos^2\theta_2 + \varepsilon_{n+1,p}\sin^2\theta_2)\sin^2\theta_1$ and $t_n = 1/4\,(\varepsilon_{n+1,f} - \varepsilon_{n+1,p})\,\sin(2\theta_1)\,\sin(2\theta_2)e^{i(\varphi_1+\bar\varphi_1-\varphi_2+\bar\varphi_2)}$, where we use the fully entangled basis labels as $p = a^{(2)}$ and $f = b^{(2)}$. We can see that the angles φ_i and $\bar\varphi_i$ only change the overall global phase of the hoppings and can thus be set to 0, so that there are only two relevant LUT manifold angles left. Moreover, since $\varepsilon_{n,p}$ and $\varepsilon_{n,f}$ are uncorrelated random numbers, it follows from Eq. (4) that disorder-averaged properties are symmetric with respect to $\theta_i \to \pi/2 - \theta_i \to \pi/2 + \theta_i$, and thus it suffices to consider $\theta_i \in [0, \pi/4]$. We have scanned the entire angle control parameter space and observed that the strongest enhancement of the average PN is obtained for $\theta_1 = \theta_2 = \pi/4$. For presentation purposes we set $\theta \equiv \theta_1 = \theta_2$.

In the absence of disorder the PN of a CLS is equal to 1 in the FD basis. In contrast the average PN of the eigenstates $\langle\text{PN}\rangle$ differs significantly from this CLS result, as shown in Fig. 2(a). The absolute maximum is reached for $\theta = \pi/4$, which maximizes the hopping matrix elements in Eq. (4). The energy dependence of the average PN shows that the largest values are obtained at the flat-band energy, as shown in the inset of Fig. 2(a). However, even in this case the average PN remains constant with the increase of the system size ($\alpha \approx 0$), indicating localized eigenstates [35].

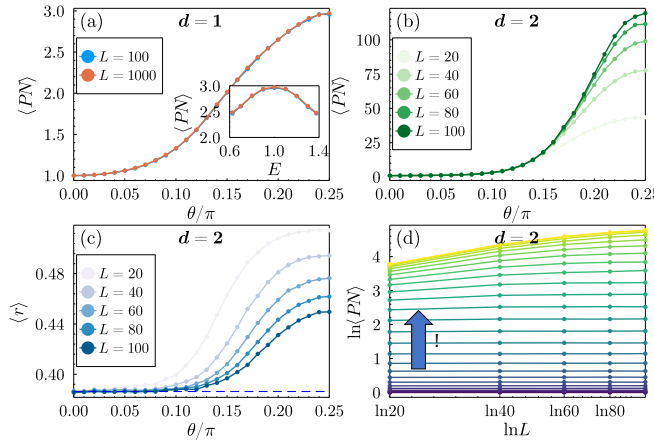

FIG. 2. Weakly disordered ABF in $d = 1$ and 2. Numbers of unit cells used are L and L^2 for $d = 1$ and $d = 2$, respectively. (a) Average participation number $\langle\text{PN}\rangle$ of the 1D effective model (4) as a function of the manifold angle θ. Inset: Energy dependence of $\langle\text{PN}\rangle$ for $\theta = \pi/4$, where the flat-band energy is equal to 1. All the other panels refer to the $d = 2$ case. (b) $\langle\text{PN}\rangle$ for the effective model as a function of θ. (c) Average ratio of adjacent gaps for different manifold angles θ. With the increasing system size the average ROAG tends to its Poisson value, indicated by a dashed blue line. (d) Scaling of $\langle\text{PN}\rangle$ with the system size $\langle\text{PN}\rangle \sim L^\alpha$, θ increases from 0 to $\pi/4$ from bottom to top along the arrow direction. The exponent $\alpha \to 0$ for larger system sizes for all values of θ.

Similarly to the one-dimensional case we construct the scale-free model in two dimensions. It corresponds to the two-dimensional Anderson model with correlated on-site energies and hopping. The $d = 2$ scale-free model has all eigenstates being localized for all θ, although we observe much stronger finite size effects as compared to $d = 1$. As in $d = 1$ we present results for a reduced number of manifold angles by choosing $\theta \equiv \theta_1 = \theta_2 = \theta_3$ and set $\varphi_i = \bar\varphi_i = 0$ and observe that the maximum average PN is reached for $\theta = \pi/4$ [see Fig. 2(b)]. The localization is confirmed by observing that the finite size scaling of the exponent α of the average PN is vanishing, as can be seen in Fig. 2(d). We also analyze the localization properties through spectral statistics analysis and the ratio of adjacent gaps [36,37] (ROAG). The latter is calculated from the consecutive level spacing $s_i = E_i - E_{i-1}$, where the set of energies E_i is ordered by their ascending value. The ROAG is then given as $r_i = \min(s_i, s_{i+1})/\max(s_i, s_{i+1})$ and its distributions can be compared to the random matrix theory predictions [36,37]. For ergodic systems the average ROAG $\langle r\rangle$ is given by a value determined by the symmetry class of the system, while in the localized regime $\langle r\rangle \sim 0.386$, corresponding to the Poisson distribution of energies. As shown in Fig. 2(c), we observe that the level statistics is in agreement with the Poisson distribution of energies, confirming that the eigenstates stay localized for $d = 2$.

Metal-insulator transition in $d = 3$. As in lower-dimensional cases, here we again reduce the number of LUT manifold parameters to one: $\theta \equiv \theta_i$ for $i = 1$, 2, 3, and 4.

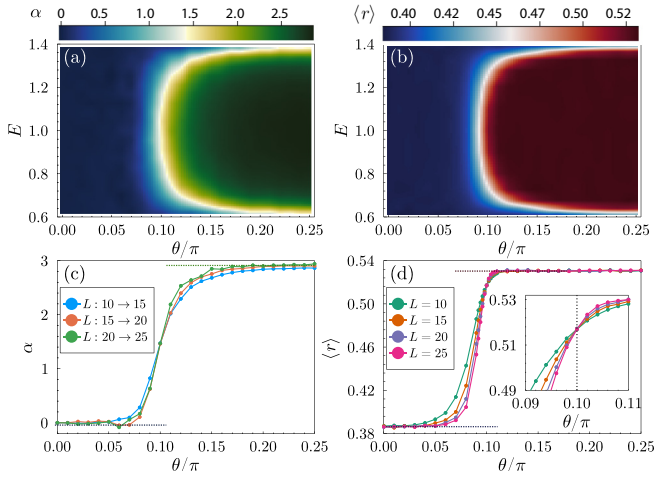

FIG. 3. Panels (a) and (b) show the energy-resolved exponent α ($\langle \mathrm{PN}\rangle \sim L^{\alpha}$) and the average ratio of adjacent gaps $\langle r\rangle$ at weak disorder as a function of the ABF manifold angle θ. Two distinct phases are clearly identified, with a white region denoting the metal-insulator transition. Panels (c) and (d) show α and $\langle r\rangle$ as a function of the manifold angle θ at the flat-band energy, respectively. The inset in panel (d) shows the zoom into the transition region which occurs at a critical value of the manifold angle, $\theta_c/\pi = 0.1$. The number of unit cells used is L^3.

The scale-free Hamiltonian is a nearest neighbor and diagonal unit cell hopping cubic lattice model, which we construct and study numerically using the ED to obtain the eigenstates and eigenenergies.

We show the energy-resolved average PN exponent α and the average ROAG as a function of the ABF manifold angle θ in Figs. 3(a) and 3(b), respectively. The results clearly show two distinct regions: first with $\langle \mathrm{PN}\rangle$ not scaling with system size ($\alpha \to 0$) and $\langle r\rangle \sim 0.386$, which correspond to localized eigenstates and Poisson distribution of energies; and second with $\langle \mathrm{PN}\rangle$ increasing with the system size ($\alpha \to d = 3$) and $\langle r\rangle \sim 0.531$, corresponding to extended eigenstates and the level statistics of the Gaussian orthogonal ensemble. Thus we identify the former as an insulator and the latter as a metal. From Figs. 3(a) and 3(b) we also observe a mobility edge—the states at the band edge and the center of the band are localized and extended, respectively. Figures 3(c) and 3(d) show the exponent α and the average ROAG as a function of the ABF manifold angle at the flat-band energy for different system sizes, confirming the existence of the metal-insulator transition in the weakly perturbed three-dimensional ABF system, driven by varying the ABF manifold parameter.

Conclusions. In this work we have studied all band flat systems in the presence of weak on-site potential disorder. Our construction of ABF systems in the continuous manifold of LUT angles enables a systematic study of effects of perturbations. By constructing the scale-free models we explain the independence of localization properties for the weak disorder in ABF systems. We demonstrate that in the cases of $d = 1$ and $d = 2$, two-band ABF systems, the eigenstates are always localized. In the case of $d = 3$ ABF lattices at infinitesimal disorder we observe a metal-insulator transition, driven by the change in the LUT manifold angles. It follows that ABF models respond qualitatively different to infinitesimally weak perturbations, allowing for phase transitions within the ABF manifold. This substantiates the strong need to explore the manifold of flat-band models beyond the commonly known examples (e.g., Lieb and kagome lattices) to search for novel physical phenomena.

In addition to weak uncorrelated on-site disorder, weak randomizations of hoppings, weak random magnetic fields and fluxes, and weak hopping detuning off the ABF model pool can be considered as additional important perturbations which can lead to novel phases and physics. In particular the randomization of hoppings and the deviation from the ABF pool seem to be relevant issues for experimental attempts to first realize ABFs and then to perturb them. Additional perturbations—say slight detunings of the hoppings away from the ABF pool—will be characterized by an additional small energy scale V. The value of the ratio of V to the weak on-site disorder energy scale W will be decisive. If both scales are much smaller than the FB gap Δ, and if W is still much larger than V, the experimental realization is expected to demonstrate our predictions. For practical purposes it seems to suffice to request $V/\Delta \leqslant 10^{-2}$ and $W/\Delta \approx 10^{-1}$.

The approach used and the results obtained in this work generalize to the case of $\nu > 2$ all bands flat lattices, with ν distinct $U = 1$ flat bands, or models with a mixture of dispersive and $U = 1$ flat bands, provided the flat bands are gapped away from the other bands and the gap is much larger than the disorder strength. The latter condition ensures that the disorder can be treated as *weak*. The $U = 1$ flat bands can all be generated with LUTs [20]. Then the effective model (3) description is valid and is derived following the steps outlined above, e.g., using the projection P_a on the flat band. Therefore, results similar to the above are expected in these model generalizations: no metallic phase in $d = 1$ and 2, and a metal-insulator transition in $d = 3$. The presence and the details of the transition will depend on the details of the LUTs used. For other gapped flat bands with nonorthogonal CLS sets ($U > 1$), the scale-free model can still be constructed using the projector P_a on the flat band. However, the projector might no longer be compact and show exponentially decaying entries. That is expected to produce disorder with exponentially decaying correlations in the scale-free model, which again should not affect the predictions qualitatively [38]. The results are expected to change qualitatively in the case of flat bands with band touchings to dispersive bands, when the CLS set ceases to be linearly independent and complete [23]. Finally an interesting question is how different flat-band systems react to infinitesimal quasiperiodic disorder, which is a subject of ongoing work.

In the past years remarkable experimental progress has been achieved with realizations and manipulations of flat-band systems in superconducting networks, engineered atomic lattices, cold-atomic systems, femtosecond laser written waveguide arrays, optically induced lattices, and exciton-polariton condensates (for recent reviews see Refs. [4,5]). In the context of fine-tuning and designing of various tight-binding models, cold atoms in optical lattices represent an outstanding physical platform. Using either stationary lattices or Floquet engineering [39,40], various lattice systems have been realized, such as a one-dimensional two-band flat-band

system—the Creutz ladder [41,42]—and the two-dimensional kagome [43] and Lieb [44] lattices. Furthermore synthetic gauge fields were realized experimentally, e.g., with the Haldane model [45] as well as with fine-tuned interactions to realize a three-dimensional Hubbard model [46]. Localization and metal-insulator transitions were also studied experimentally in $d = 1$ optical lattices with uncorrelated [47] and correlated [48,49] on-site disorder, respectively. Experimental observations of the Anderson transition [50] are also feasible with a driven $d = 1$ system with several incommensurate frequencies to generate additional synthetic lattice dimensions [51]. The high tunability of the experimental platforms suggests that localization phenomena in flat-band systems such as the ones we discuss in this work can be experimentally realized and studied.

Acknowledgments. T.Č. and Y.K. have contributed equally to this work. T.Č. acknowledges fruitful discussions with Carlo Danieli. The authors gratefully acknowledge the support by the Institute for Basic Science in Korea (Project No. IBS-R024-D1).

[1] O. Derzhko, J. Richter, and M. Maksymenko, Int. J. Mod. Phys. B **29**, 1530007 (2015).
[2] S. A. Parameswaran, R. Roy, and S. L. Sondhi, C. R. Phys. **14**, 816 (2013).
[3] E. J. Bergholtz and Z. Liu, Int. J. Mod. Phys. B **27**, 1330017 (2013).
[4] D. Leykam, A. Andreanov, and S. Flach, Adv. Phys.: X **3**, 1473052 (2018).
[5] D. Leykam and S. Flach, APL Photonics **3**, 070901 (2018).
[6] B. Sutherland, Phys. Rev. B **34**, 5208 (1986).
[7] H. Aoki, M. Ando, and H. Matsumura, Phys. Rev. B **54**, R17296 (1996).
[8] A. Mielke, J Phys. A: Math. Gen. **24**, L73 (1991).
[9] H. Tasaki, Phys. Rev. Lett. **69**, 1608 (1992).
[10] A. Mielke and H. Tasaki, Commun. Math. Phys. **158**, 341 (1993).
[11] A. P. Ramirez, Annu. Rev. Mater. Sci. **24**, 453 (1994).
[12] S. Peotta and P. Törmä, Nat. Commun. **6**, 8944 (2015).
[13] A. Julku, S. Peotta, T. I. Vanhala, D.-H. Kim, and P. Törmä, Phys. Rev. Lett. **117**, 045303 (2016).
[14] M. Tovmasyan, S. Peotta, L. Liang, P. Törmä, and S. D. Huber, Phys. Rev. B **98**, 134513 (2018).
[15] R. Mondaini, G. G. Batrouni, and B. Grémaud, Phys. Rev. B **98**, 155142 (2018).
[16] H. Aoki, J. Supercond. Novel Magn. **33**, 2341 (2020).
[17] Y. Kuno, T. Orito, and I. Ichinose, New J. Phys. **22**, 013032 (2020).
[18] C. Danieli, A. Andreanov, and S. Flach, Phys. Rev. B **102**, 041116(R) (2020).
[19] P. Anderson, Phys. Rev. **109**, 1492 (1958).
[20] S. Flach, D. Leykam, J. D. Bodyfelt, P. Matthies, and A. S. Desyatnikov, Europhys. Lett. **105**, 30001 (2014).
[21] J. Vidal, P. Butaud, B. Douçot, and R. Mosseri, Phys. Rev. B **64**, 155306 (2001).
[22] S. Nishino, H. Matsuda, and M. Goda, J. Phys. Soc. Jpn. **76**, 024709 (2007).
[23] J. T. Chalker, T. S. Pickles, and P. Shukla, Phys. Rev. B **82**, 104209 (2010).
[24] D. Leykam, S. Flach, O. Bahat-Treidel, and A. S. Desyatnikov, Phys. Rev. B **88**, 224203 (2013).
[25] D. Leykam, J. D. Bodyfelt, A. S. Desyatnikov, and S. Flach, Eur. Phys. J. B **90**, 1 (2017).
[26] A. Ramachandran, A. Andreanov, and S. Flach, Phys. Rev. B **96**, 161104(R) (2017).
[27] P. Shukla, Phys. Rev. B **98**, 054206 (2018).
[28] M. Goda, S. Nishino, and H. Matsuda, Phys. Rev. Lett. **96**, 126401 (2006).
[29] C. Danieli, A. Andreanov, T. Mithun, and S. Flach, Phys. Rev. B **104**, 085131 (2021).
[30] M. Creutz, Phys. Rev. Lett. **83**, 2636 (1999).
[31] P. Sathe, F. Harper, and R. Roy, J. Phys. A: Math. Theor. **54**, 335302 (2021).
[32] F. Wegner, Z. Phys. B: Condens. Matter **36**, 209 (1980).
[33] C. Castellani and L. Peliti, J. Phys. A: Math. Gen. **19**, L429 (1986).
[34] F. Evers and A. D. Mirlin, Rev. Mod. Phys. **80**, 1355 (2008).
[35] Localization in $d = 1$ is further confirmed by calculating the ratio of adjacent gaps, which corresponds to the Poisson distribution of energies (not shown). We have also calculated the localization length using the transfer matrix method and the results agree with the results for the PN (not shown).
[36] V. Oganesyan and D. A. Huse, Phys. Rev. B **75**, 155111 (2007).
[37] Y. Y. Atas, E. Bogomolny, O. Giraud, and G. Roux, Phys. Rev. Lett. **110**, 084101 (2013).
[38] F. M. Izrailev, A. A. Krokhin, and N. Makarov, Phys. Rep. **512**, 125 (2012).
[39] A. Eckardt, Rev. Mod. Phys. **89**, 011004 (2017).
[40] T. Oka and S. Kitamura, Annu. Rev. Condens. Matter Phys. **10**, 387 (2019).
[41] J. H. Kang, J. H. Han, and Y. Shin, New J. Phys. **22**, 013023 (2020).
[42] Y. He, R. Mao, H. Cai, J.-X. Zhang, Y. Li, L. Yuan, S.-Y. Zhu, and D.-W. Wang, Phys. Rev. Lett. **126**, 103601 (2021).
[43] G.-B. Jo, J. Guzman, C. K. Thomas, P. Hosur, A. Vishwanath, and D. M. Stamper-Kurn, Phys. Rev. Lett. **108**, 045305 (2012).
[44] S. Taie, H. Ozawa, T. Ichinose, T. Nishio, S. Nakajima, and Y. Takahashi, Sci. Adv. **1**, e15000854 (2015).
[45] G. Jotzu, M. Michael, D. R. emi, L. Martin, U. Thomas, G. Daniel, and E. Tilman, Nature (London) **515**, 237 (2014).
[46] R. A. Hart, P. M. Duarte, T.-L. Yang, X. Liu, T. Paiva, E. Khatami, R. T. Scalettar, N. Trivedi, D. A. Huse, and R. G. Hulet, Nature (London) **519**, 211 (2015).
[47] J. Billy, V. Josse, Z. Zuo, A. Bernard, B. Hambrecht, P. Lugan, D. Clément, L. Sanchez-Palencia, P. Bouyer, and A. Aspect, Nature (London) **453**, 891 (2008).
[48] G. Roati, C. D'Errico, L. Fallani, M. Fattori, C. Fort, M. Zaccanti, G. Modugno, M. Modugno, and M. Inguscio, Nature (London) **453**, 895 (2008).
[49] H. P. Lüschen, S. Scherg, T. Kohlert, M. Schreiber, P. Bordia, X. Li, S. Das Sarma, and I. Bloch, Phys. Rev. Lett. **120**, 160404 (2018).
[50] J. Chabé, G. Lemarié, B. Grémaud, D. Delande, P. Szriftgiser, and J. C. Garreau, Phys. Rev. Lett. **101**, 255702 (2008).
[51] G. Casati, I. Guarneri, and D. L. Shepelyansky, Phys. Rev. Lett. **62**, 345 (1989).